THE EFFECT OF INLET SWIRL ON THE DYNAMICS OF LONG ANNULAR SEALS IN CENTRIFUGAL PUMPS

M. Ismail and R.D. Brown
Heriot-Watt University
Edinburgh, United Kingdom

and

D. France
Weir Pumps Ltd.
Glasgow, Scotland

This paper describes additional results from a continuing research program which aims to identify the dynamics of long annular seals in centrifugal pumps. A seal test rig designed at Heriot-Watt University and commissioned at Weir Pumps Research Laboratory in Alloa permits the identification of mass, stiffness, and damping coefficients using a least-squares technique based on the singular value decomposition method. The analysis is carried out in the time domain using a multifrequency forcing function. The experimental method relies on the forced excitation of a flexibly supported stator by two hydraulic shakers. Running through the stator embodying two symmetrical balance drum seals is a rigid rotor supported in rolling element bearings. The only physical connection between shaft and stator is the pair of annular gaps filled with pressurised water discharged axially. The experimental coefficients obtained from the tests are compared with theoretical values.

1. INTRODUCTION

Research conducted in the last decade has shown that the overall rotor dynamic behaviour of centrifugal pumps is dominated by the interaction between the pumped fluid and the pump itself. Experimental evidence suggests that a pump rotor may become dynamically unstable in presence of fluid forces. As a result, the annular clearances inside the pump tend to experience excessive wear which consequently leads to increased vibration amplitude.

To avoid such problems, pump users and manufacturers have begun to adopt new specifications based on accurate prediction of rotor dynamic performance in terms of amplitude response and stability. A complete dynamic analysis of a rotating machine involves calculations of stability, damped natural frequencies and response of the system to excitation forces. Accurate predictions require that all important mechanical components such as bearings and annular seals be represented with regard to their dynamic characteristics.

The dynamic behaviour of neck-ring and interstage seals has been well established using a linear theory. Considerable research has been done with respect to these seals and the theory has been confirmed by experimental data as far as short seals are concerned. However, theoretical models for long seals typical of a balance drum are less satisfactory and there is a dearth of experimental data which is usually obtained from small scale test rigs which do not represent geometric configurations of flow regimes found in modern centrifugal pumps. As a result, the effect of fluid forces in long seals on the performance and dynamic behaviour of centrifugal pumps are not well understood.

The work reported here was supported by S.E.R.C. and Weir Pumps Ltd and aims to identify the dynamics of long annular seals in centrifugal pumps. The detailed design of the test rig was described in (1). A general layout of the test facility including measurement pick-ups is shown in

figure 1. The test rig situated at Weir Pumps Research Laboratory at Alloa consists of a rigid shaft supported by rolling bearings at both ends and a very rigid housing mounted on coil springs. (initially, the casing was mounted on air bellows). A pair of simulated balance drum test seals is installed in the housing and water is charged from the centre of the casing and discharged from both ends. A significant feature of the flow path is the radial inward motion before entry to the annular clearance space. Two hydraulic actuators offset spatially at 90° are used to apply forces to the middle of the casing. Figure 2 shows a schematic view of the primary test section and figure 3 shows some details of the rotor and seals. The oscillatory motion of the casing, when excited by external forces is modified by the dynamic characteristics of the flow passing through the seals.
A linearised mathematical model is generally the appropriate starting point to study dynamic forces in pump annular seals. Hence the following model was assumed for the seal reaction forces:

$$\begin{Bmatrix} R_x \\ R_y \end{Bmatrix} = \begin{bmatrix} K_{xx} & K_{xy} \\ K_{yx} & K_{yy} \end{bmatrix} \begin{Bmatrix} x \\ y \end{Bmatrix} + \begin{bmatrix} C_{xx} & C_{xy} \\ C_{yx} & C_{yy} \end{bmatrix} \begin{Bmatrix} \dot{x} \\ \dot{y} \end{Bmatrix} + \begin{bmatrix} M_{xx} & 0 \\ 0 & M_{yy} \end{bmatrix} \begin{Bmatrix} \ddot{x} \\ \ddot{y} \end{Bmatrix}$$

Here K, C, and M are the stiffness, damping, and inertia matrices of the fluid as it passes through the clearance space and (x,y) is the instantaneous displacement vector of the seal stator relative to the rotor.
Following the commissioning stage of the test rig, preliminary tests were carried out for moderate pressures and rotor speeds and the obtained results were presented in (2). These results showed good agreement between theoretical and experimental direct and cross-coupled stiffness coefficients. However, experimental direct damping coefficients showed large discrepancies when compared with theoretical values. While the theory predicts an increase in damping with increasing pressure, the experimental results showed no discernible increase in damping. Cross-coupling damping and to a lesser extent fluid inertia could not be estimated accurately. On the other hand, measured radial pressure distributions lead to inlet swirl ratios of about 0.8 to 1.0 as compared to the commonly assumed value of 0.5 .
Now although these preliminary results were seen as very encouraging, the major drawback was that the tests could not be extended to higher pressures and higher rotor speeds. The low stiffness of the casing suspension system resulted in flow induced vibrations which limited the testing range to a rotor speed of about 1600 rpm and a pressure of 4.5 bar. It was clear from the tests that these flow induced vibrations were associated with the rotation of the shaft because of their synchronous nature and there was strong evidence that they were caused by fluid cross-coupled forces in the seals. Using the idea of Massey (3), grooved rings were installed in the axial gap between the back shroud of the simulated impeller and the casing with the expectation that the grooves would result in a lower fluid swirl at seal entry. They were 25 radial grooves of 45 mm length, 6 mm width and 1.5 mm depth. Following this simple modification, a significant reduction in the vibration level was achieved. In fact, with this configuration the rotor could be run up to the maximum achievable speed of 3000 rpm (limited by the DC. motor) at any pressure up to 15.7 bar (limited by the delivery pump) with peak displacements not exceeding 25 μm. It is well known that a reduction of swirl at seal entry results in a reduction of the fluid cross-coupled forces. It is thus obvious that the vibrations experienced without the grooves are a direct result of fluid cross-coupling in the seals. Since the test rig design enabled different test rings to be tested, it was possible to investigate the effect of various groove designs on the dynamic behaviour of the system.

The results presented in this paper are for a pair of seals and are mainly concerned with grooved plates. Modifications to the hardware and software reported in (2) are summarised in section 2. The radial pressure distribution measurements and swirl ratios are discussed in section 3. The measured and theoretical dynamic characteristics of the seals are presented and discussed in section 4.

2. HARDWARE, DATA ACQUISITION AND SOFTWARE

2.1. Hardware

One of the major problems that affected the progress of this work was associated with the hydraulic servo-actuators which provided the exciting forces. The original system worked well at the low speed and pressure limits of the plain test rings. However the system degraded over time, mainly due to the fact the original servo-valves were over-sized and unduly sensitive to wear. In addition the air suspension system was inadequate at the higher speeds made possible by the grooved test rings. The system was modified by changing the casing suspension to a coil spring system , using better quality ball bearings for rotor support and installing servo-valves with a lower flow requirement to suit the very small motions of the casing. The overall stiffness of the coil springs was 900 N/mm considerably less than the expected seal stiffness. The overall behaviour was much improved and it became possible to test throughout the entire range of speed and pressure available.

2.2 . Data Acquisition and signal processing

The instrumentation system detailed in (2) allows for high speed sampling of 12 channels at an overall sampling rate of 30 000 samples/s. These channels consisted of 6 displacement (2 relative), 4 acceleration and 2 force transducers. The absolute accelerations and displacements provide data to confirm that the forced motion of the casing is parallel to the shaft while the relative displacements check that there is no significant movement of the shaft. The forces generated by the hydraulic jacks are controlled by two digital-to-analogue multi-frequency signals which have been synthesised in the computer and stored in the data acquisition unit. In addition to the data sampling, the data acquisition unit is also used to convert the digital forcing signals into analogue ones.
The number of samples recorded for each channel has been increased from 2048 (2) to 15706. As a result a significant reduction in the variance of the estimated coefficients was achieved. Variance is a measure of the scatter in the experimental results.
Worden (12) has shown that estimation of the parameters of a linear system is not possible for single frequency excitation due to linear dependence of the state vectors. However, multi-frequency excitation can yield a large population of state vectors to provide the data set for a least squares optimisation, while avoiding these linear dependencies. In this case the singular value decomposition (SVD) method (2,12,13) was used to assess the significance of any term in the linear model. In order to minimise any contact between shaft and casing a low peak factor algorithm (14) was used to select the phase for the four excitation frequencies of 19, 25, 34 and 43 Hz. The test shaft speeds were chosen so as to avoid these frequencies.
Once a reliable data set had been obtained there was some signal processing involved before the analysis could commence. This consisted of mean removal, band pass filtering and notch filtering to remove any synchronous component. In addition velocity data had to be obtained from a numerical procedure. An estimated velocity vector was formed by integrating the acceleration

values, differentiating the displacement values, and taking the average. The processed data was then used to produce estimates of all the coefficients in the linear model and the appropriate standard errors. A data acquisition and reduction flow chart is shown in figure 4. More details are given by Brown and Ismail (2).

3. SWIRL MEASUREMENTS

3.1. Introduction

The equilibrium equation in the radial direction, in the axial gap h made the simulated impeller and the casing (figure 3) is given by:

$$-V_r \frac{dV_r}{dr} - \frac{v_t^2}{r} = -\frac{1}{\rho}\frac{dp}{dr} + \frac{\tau_{rwall}}{\rho h} \pm \frac{\tau_{rdisk}}{\rho h}$$

Neglecting the radial shear stresses τ_{rwall} and τ_{rdisk} and neglecting the change in radial velocity, the above equation becomes:

$$\frac{dp}{dr} = \frac{\rho v_t^2}{r} = \rho r \omega^2$$

where ω is the fluid angular velocity at radius r. Stepanoff (4) gives results of the integration of the above equation for a velocity distribution given by an equation of the form:

$$\omega = Cr^m$$

where C and m are constants, m = 2 for a free vortex and m = 0 for a forced vortex. The well known free and forced vortex are special cases of vortex motion.
The fluid angular velocity at seal inlet is obtained from the measured radial pressure distribution. For instance, in the case of a forced vortex we have:

$$p(r) = \int dp = \rho\omega^2 \int r dr$$

If the pressure is known at a radius r_1 and at seal inlet (r=R), integration of the above equations yields the fluid angular velocity at seal inlet

$$\omega = \sqrt{\frac{2}{\rho}\frac{p(R) - p(r_1)}{R^2 - r_1^2}}$$

3.2. Radial pressure distribution and fluid swirl at inlet : Results and discussion

The study of the radial pressure distribution of the flow in the gap between the back of the simulated impeller and the casing involved the measurement of the differential pressure at five radial positions (figure 3) for various flow rates and shaft speeds. A non dimensional flow coefficient C_q defined as :

$$Cq = \frac{Q}{\Omega R_2^2 h}$$

was used to analyse the results.

A comparison of swirl measurement results obtained in this work with those directly measured by Addlesee et al (5) for both the plain and the grooved plates is shown in figure 5. Addlesee et al used a Laser Doppler Anemometer to measure the velocity distribution in the gap between two coaxial disks simulating the entrance region of a balance drum seal. Figure 5 shows close agreement between the results obtained from the two different methods although the LDA measurements gave lower swirl values for the plain plates and higher swirl values with the grooves. This difference could be due to a different gap width and is consistent with further measurements (5) which showed that larger gaps lead to a decrease in swirl for the plain plates and an increase in swirl for the grooved plates. Hence, it can be argued that as the gap width increases the grooves become less effective. But it is obvious that the grooves reduce the swirl considerably, about 50 % for low values of C_q that is for high shaft speeds. It is also clear that higher leakage leads to higher swirl implied by a greater fluid total velocity.

4. DYNAMIC COEFFICIENTS

4.1. System coefficients without water

As the test rig only allowed total coefficients to be extracted, the stiffness and damping of the system without water had to be measured. For the grooved plate configuration the overall stiffness was 1.45 MN/m, slightly more than the stiffness of the coil springs alone. This is probably due a combined effect of the lateral stiffness of the springs and the supply hoses. Impact testing using a force hammer gave decay traces which were analysed. The damping coefficient was about 5000 Ns/m, about 10% of the seal direct damping.

4.2. Seal dynamic coefficients

The dynamic coefficients of the test seals were measured at four different flow rates and six shaft speeds, covering a range of 720 to about 3000 rpm. The axial Reynolds number varied from about 6900 to 12100 and the circumferential Reynolds number varied from about 1200 to 6000. In addition to the dynamic tests, some static and impact tests were also carried out in order to check the validity of the data. The experimental coefficients are compared to theoretical values based on Black's theory (9-11). The cross-coupled stiffness is calculated using the measured swirl as explained in (2).

4.2.1 Direct stiffness coefficients

After allowing for the stiffness of the system without water, the experimental direct stiffness coefficients of the seals are plotted in figure 6.a and 6.b . The theoretical coefficients are also plotted for comparison with the experiment. From these figures, it can be clearly seen that the major effect is an increase of stiffness with increasing axial Reynolds number. The theory predicts a symmetric stiffness for a centred seal but the experimental data shows some scatter. This is probably due to small eccentricities since the sampled data corresponds to small displacements around a centred position. The figures also show that while the theory predicts a decrease in stiffness with increasing shaft speed, the test data indicates that the direct stiffness is independent on shaft speed. There is some scatter in the test data but no discernible trend can be observed. The theoretical stiffness is given by the following expression:

$$K = \frac{\pi R \Delta p}{\lambda}\left(\mu o - \frac{1}{4}\mu_2 \Omega^2 T^2\right)$$

If the shaft speed is increased while the flow rate is kept constant, the change in stiffness in the above expression is mainly influenced by the second term which contains μ_2, that is the fluid inertia coefficient. However, published experimental work has shown that this term is generally over-estimated by the theory. The plotted data also shows that the theory under-estimates the stiffness by about 20 to 25%. A direct measurement (static test) of stiffness for no rotation is shown in Figure 6.c . It is clear that the values are comparable with the identified stiffness.

4.2.2. Cross-coupled stiffness coefficients

The theoretical and experimental cross-coupled stiffness coefficients are shown in figure 7. As predicted by the theory, the experimental coefficients increase linearly with the shaft speed. The sign of the coefficients is also detected accurately. There is good agreement between theory and experiment at low axial Reynolds number, figure 7.a, the theory overpredicting the coefficients by about 10%. But when the axial Reynolds number increases the agreement deteriorates. The theory predicts larger coefficients than the experimental ones especially at high shaft speeds, figure 7.b. For this case, the predicted coefficients are about twice as large as the experimental ones. In order to explain this discrepancy some of the theoretical assumptions were reviewed.
The theoretical stiffness expression is based on a model that assumes that (i) the seal is concentric, (ii) the rotating and stationary walls of the seal have the same surface roughness and (iii) the circumferential fluid velocity starts from an arbitrary initial swirl and asymptotically approaches $0.5R\Omega$ as it proceeds axially along the seal. In (6), Childs and Kim used a combined analytical-computational method to predict the fluid circumferential velocity in seals which may have different surface roughness treatments on the stator or rotor seal elements. They predicted that the circumferential velocity solution in a seal with the same rotor and stator roughness converges asymptotically towards $0.5R\Omega$ irrespective of whether both wall surfaces are smooth or rough. However, they predicted an asymptote less than $0.5R\Omega$ if the stator is rougher than the rotor and greater than $0.5R\Omega$ if the rotor is rougher than the stator. Further evidence that the fluid circumferential velocity inside a seal can be different from $0.5R\Omega$ was provided by Addlesee et al (5). Addlesee et al used a specially designed test rig to study the distribution of fluid velocity at different axial positions in a rotating annulus utilising an LDA technique. The test results reported in (5) suggest that the fluid circumferential velocity is strongly dependent on the inlet swirl. Specifically, strong inlet swirl gave high circumferential velocities (greater than $0.5\ R\Omega$) and weak inlet swirl gave low circumferential velocities (less than $0.5\ R\Omega$). On the other hand, the fluid cross-coupled stiffness varies proportionally with the fluid circumferential velocity. Since the inlet swirl in this work can be considered as weak and that the stator surface roughness is greater than the rotor surface roughness (1.5 μm and 0.5 μm), it can be argued that the discrepancy between theoretical and experimental cross-coupled stiffness coefficients is the result of a combined effect of a rougher stator and a reduced fluid circumferential velocity. This view was supported by a good correlation between predicted and measured cross-coupled stiffness coefficients when smaller values of fluid circumferential velocities were assumed. Larger discrepancies between predicted and measured cross-coupled stiffness coefficients at the higher speeds are consistent with flow measurements which showed that higher speeds lead to smaller inlet swirl ratios, resulting in

smaller values for the fluid circumferential velocity. An other factor that contributes to the reduction in fluid circumferential velocity is the axial velocity of the flow. When the fluid enters the seal with an initial swirl, the axial pressure drop imposes an axial velocity component on the flow which then proceeds in the seal with a combined peripheral and axial motion. But as the axial velocity increases, the passage time T becomes smaller and the fluid motion becomes dominated by the axial velocity. As a result, a fluid particle entering the seal with some initial swirl may exit it with little peripheral motion or more specifically with a weaker peripheral motion than in the case of a larger passage time.

4.2.3 Direct damping coefficients

The experimental and theoretical direct damping coefficients are shown in figure 8 for R_a values of 6950 and 12 120. As predicted by the theory, the direct damping does not vary with shaft speed. The theoretical and experimental coefficients coincide at low axial Reynolds number but disagree at high axial Reynolds number. The experimental data indicates that the damping is almost insensitive to changes in Reynolds number, which is in contradiction with the theory. It is worthwhile noting that similar discrepancies between theoretical and experimental direct damping coefficients were also reported by Childs et al in (6), (7) and (8). In (6), Childs and Kim reported that measured damping coefficients were smaller than the theoretical ones at low axial Reynolds number but as the Reynolds number increased the agreement between theory and experiment improved.

4.2.4 Overall dynamic behaviour

The linear modelling of the complete system was tested by comparing the simulated exciting forces from the linear model with the experimentally measured forces from the two hydraulic jacks. As can be seen from figure 9 the comparison demonstrates that an overall RMS error of 16% gives a very good reproduction of the forces acting on the casing. Thus the linear model is shown to be capable of predicting vibration response accurately.

5. CONCLUSIONS

Extensive testing with the grooved plates allowed a constructive critical review of the theoretical model to be made. Reassessment of the theoretical assumptions was made possible by carrying out tests covering the span of the flow rate range permitted by the supply pump. Testing at different flow rate values allowed some of the flow underlying phenomena to be unravelled. The obtained results are summarised in the following section:

- The inlet swirl ratio ω/Ω increases with the flow rate and decreases with the shaft speed, the sensitivity to flow rate being smaller in the high speed range.
- Radial pressure measurements in the gap between the back of the simulated impeller and the casing show pressure distributions which suggest the occurrence of a forced vortex motion, especially at high shaft speeds which is typical of modern centrifugal pumps.
- The use of radial grooves of 1.5 mm depth at the entrance to the balance drum resulted in a significant reduction in inlet swirl.
- The measurements show that only the direct stiffness, cross-coupled stiffness and direct damping coefficients are important. The cross-coupled damping coefficients were found to be insignificant as the least-squares technique gave standard errors which are larger than the

coefficients themselves. The inertia terms were identified but the scatter was large. These terms were found to lie in the range 35 to 150 Kg as compared to the theoretical value of 87 Kg. The plotted data showed no identifiable trend.

- Evidence of the beneficial effect of the grooves was noticed early when the dynamic instability experienced with the plain plates was completely suppressed. Later, experimental measurements of the dynamic characteristics of the seals showed a significant decrease in cross-coupled stiffness with the 1.5 mm deep grooved plates.
- The cross-coupled stiffness coefficients were fairly well predicted by the theory at low flow rates and small groove depth but the agreement between theory and experiment deteriorated with the increase of flow rate and groove depth. The theoretical model was reassessed by assuming that the fluid circumferential velocity in the seal is much smaller than half shaft speed.
- The direct stiffness coefficients were found to be under-predicted by the theory by about 20 to 30% in general and were found to be insensitive to swirl reductions. The measured coefficients are supported by those obtained from direct static tests.
- The measured direct damping coefficients were found to be insensitive to shaft speed, flow rate and swirl reductions. This is in serious discrepancy with the theory which predicts an increase in damping with increasing flow rate. However, impact tests carried out at the highest flow rate showed extremely good agreement with the identified damping.

Finally, it is to be noted that all identified coefficients except the cross-coupled damping terms were identified with small standard errors. The calculated root-mean square errors (RMSE) between the measured forces and those obtained by fitting the experimental data to a ten-coefficient model were of the order of 8 to 20%. The RMSE is defined as

$$RMSE(f) = 100 \times \left[\sum_{i=1}^{N} \sqrt{\frac{\left(f_i - \hat{f}_i\right)^2}{N \sigma_f^2}} \right]$$

where f is the measured force vector, $\hat{f}$ the force vector predicted by the model, σ_f the standard deviation of the measured force and N is the number of sample points in the data records. The RMSE provides a measure of the goodness of fit between the experimental data and the theoretical model.

6. REFERENCES

(1) Brown, R. D., Ismail M. and Abdulrazzak, M. Fluid forces in the annular seals of high performance centrifugal pumps, IMechE seminar, "Vibrations in centrifugal pumps", London, December 11, 1990.

(2) Brown, R. D. and Ismail M. Dynamic characteristics of long annular seals in centrifugal pumps, IMechE 5th International Conference , Vibrations in Rotating Machinery, paper C432/112, Bath, September 7-10, 1992.

(3) Massey, I. C. Sub-synchronous vibration problems in high-speed, multi-stage centrifugal pumps, Proceedings of the 14th turbomachinery symposium, turbomachinery laboratories, Texas A&M University, pp. 11-16, College Station, Texas, 1985.

(4) Stepanoff A. J. Centrifugal and Axial Flow Pumps, John Wiley and Sons, INC., 1957.
(5) Addlesee, A. J., Altiparmak, D. and Pan, S. Whirl measurements on leakage flows in turbomachine models, 7th Workshop on Rotor Instability, Texas A&M University, May, 1993.
(6) Childs, D. W. and Kim, Chang-Ho Analysis and testing for rotordynamic coefficients of turbulent annular seals with different, directionally-homogeneous surface roughness treatment for rotor and stator elements, Transaction of the ASME, Vol. 107, July, 1985, pp. 296-306.
(7) Childs, S. B. and Childs, D. W. Estimation of seal bearing stiffness and damping parameters from experimental data, NASA C.P 2133, 1980.
(8) Childs, D. W. and Dressman, J. Testing of turbulent seals for rotordynamic coefficients. Proceedings of EPRI Symposium in Power Plant Feed Pumps, CHERRY HILL, NJ, June 1982 (ICPR 1984).
(9) Black, H. F. and Jenssen, D. N. Dynamic hybrid properties of annular pressure seals, Proceedings of the Journal of Mechanical Engineering, Vol. 184, 1970.
(10) Black, H. F. and Jenssen, D. N. Effects of high pressure ring seals on pump rotor vibration, Transactions of the ASME, Paper No. 71-WA/FF-38, 1971.
(11) Black, H. F., Allaire, P. E. and Barret, L. E. Inlet flow swirl in short turbulent seal dynamics, 9th International conference on Fluid sealing, Leeewenhorst, Netherlands, April 1-3, 1981.
(12) Worden, K. Parametric and non-parametric identification of nonlinearity in Structural Dynamics, Ph.D. Thesis, 1989, Department of Mechanical Engineering, Heriot-Watt University, Edinburgh.
(13) Press, W. H., Flannery, B. P., Tenkolsky, S. A. and Vettering, W. T. Numerical Recipes, The Art of Scientific Computing, Fortran Version, Cambridge University Press, Cambridge, 1989.
(14) Schroeder, M. R. Synthesis of low-peak factor signals and binary sequences with low autocorrelation, IEEE Trans. on Information Theory, pp. 85-89, January, 1970.

NOTATION

L , c , h	seal length, seal radial clearance, axial gap between wall and rotating disk
r , R , R_d ,	radial position, seal radius, simulated impeller radius
F_x , F_y	components of the external force vector in x and y directions
R_x , R_y	seal restoring forces in x and y directions
V , V_r	average fluid axial velocity, average fluid radial velocity
v_c , v_o	fluid circumferential velocity, fluid circumferential velocity at seal entrance
T	time (L/V)
K, C, m	stiffness, damping and inertia coefficients
P , Q , C_q	pressure, flow rate, flow coefficient
R_a	average axial Reynolds number, $2\rho Vc/\mu$
R_r	average circumferential Reynolds number, $\rho\Omega Rc/\mu$
λ , σ	friction factor, $\sigma = \lambda L/c$
μ , ρ	fluid Viscosity, fluid density
Δp , ξ	pressure drop across seal, inlet loss coefficient
Ω , ω	shaft angular speed, fluid angular velocity,
τ_{rwall} , τ_{rdisk}	radial wall shear stress, radial shear stress on rotating disk

DISCUSSION

Professor Childs raised a comment concerning the acceleration terms in the equations of motions. The equations of motion for the stator mass M_s can be written as

$$\begin{Bmatrix} F_x - M_s \ddot{x}_s \\ F_y - M_s \ddot{y}_s \end{Bmatrix} = \begin{bmatrix} K_{xx} & K_{xy} \\ K_{yx} & K_{yy} \end{bmatrix} \begin{Bmatrix} \Delta x \\ \Delta y \end{Bmatrix} + \begin{bmatrix} C_{xx} & C_{xy} \\ C_{yx} & C_{yy} \end{bmatrix} \begin{Bmatrix} \Delta \dot{x} \\ \Delta \dot{y} \end{Bmatrix} + \begin{bmatrix} M_{xx} & 0 \\ 0 & M_{yy} \end{bmatrix} \begin{Bmatrix} \Delta \ddot{x} \\ \Delta \ddot{y} \end{Bmatrix}$$

Here, (F_x, F_y) are the measured components of the input forces, $(\ddot{x}_s, \ddot{y}_s)$ are the measured components of the stator acceleration and $(\Delta x, \Delta y)$ are defined bellow:

$$\Delta x = x_s - x_r$$
$$\Delta y = y_s - y_r$$

where the subscripts s and r identify the stator and rotor respectively. We measure the absolute stator displacements (x_s, y_s) and the relative displacements $(\Delta x, \Delta y)$. The measured displacements show that when the synchronous noise is removed from the data we have

$$\Delta x \approx x_s$$
$$\Delta y \approx y_s$$

and hence the use of absolute accelerations is justified. The above condition is implied by the rigid rotor design used. Should this condition not be satisfied one can use a numerical procedure to obtain the relative accelerations from the measured relative displacements $(\Delta x, \Delta y)$. In fact this procedure is currently being adopted for the high pressure tests.

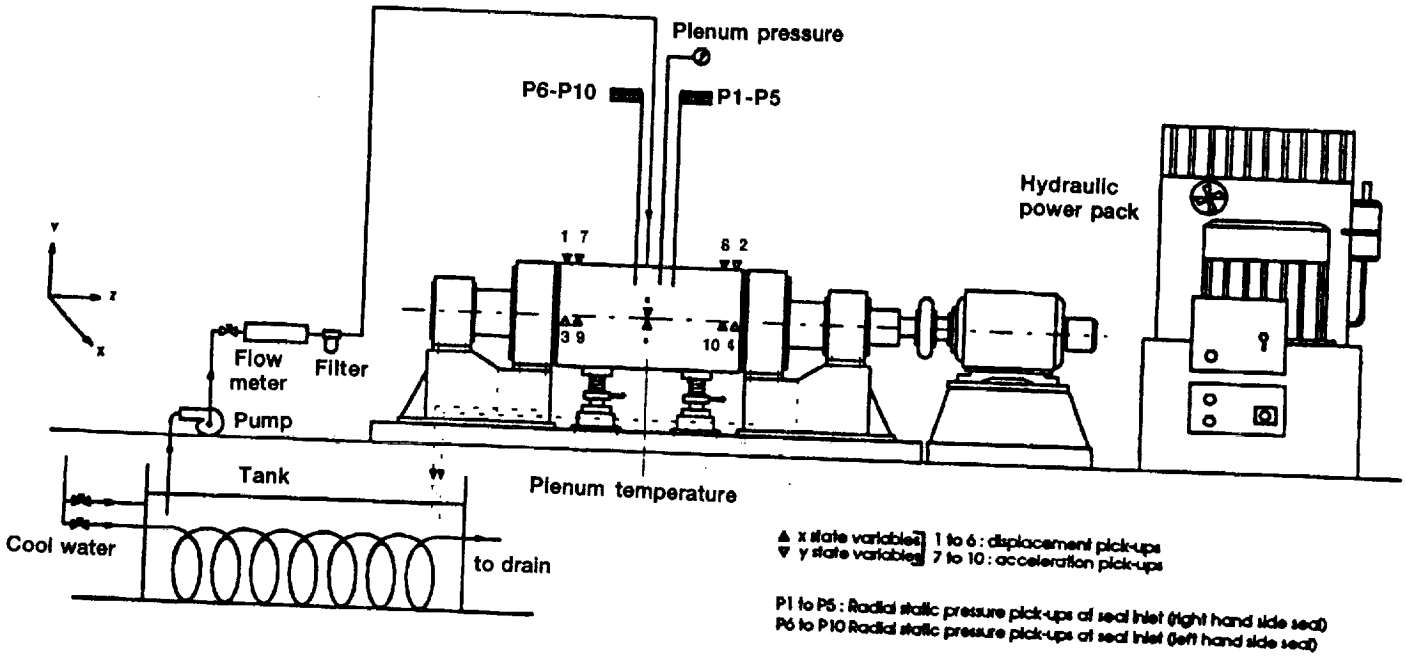

Figure 1 Test rig layout; instrumentation and hydraulic shakers not shown

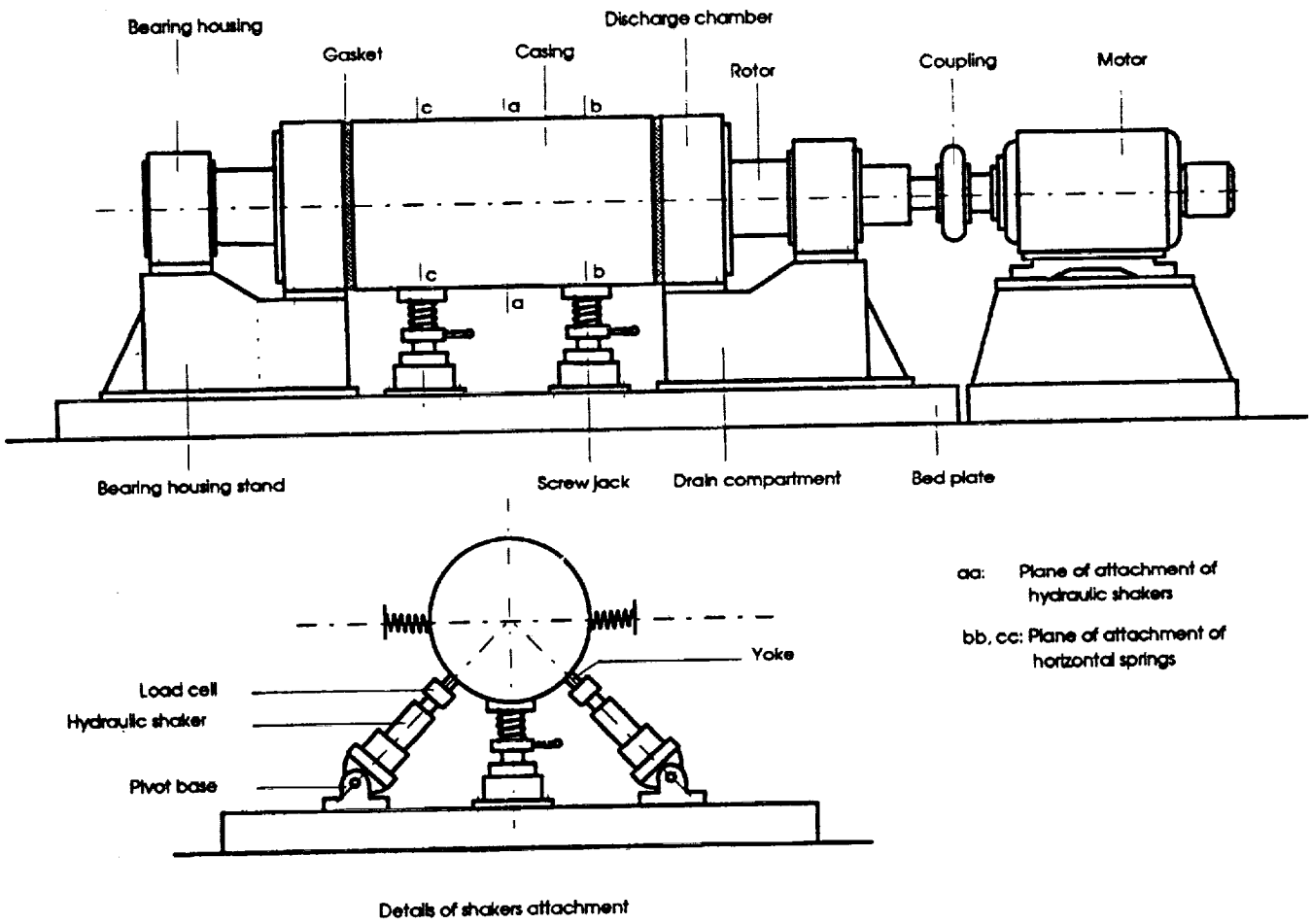

Figure 2 Schematic view of primary test section

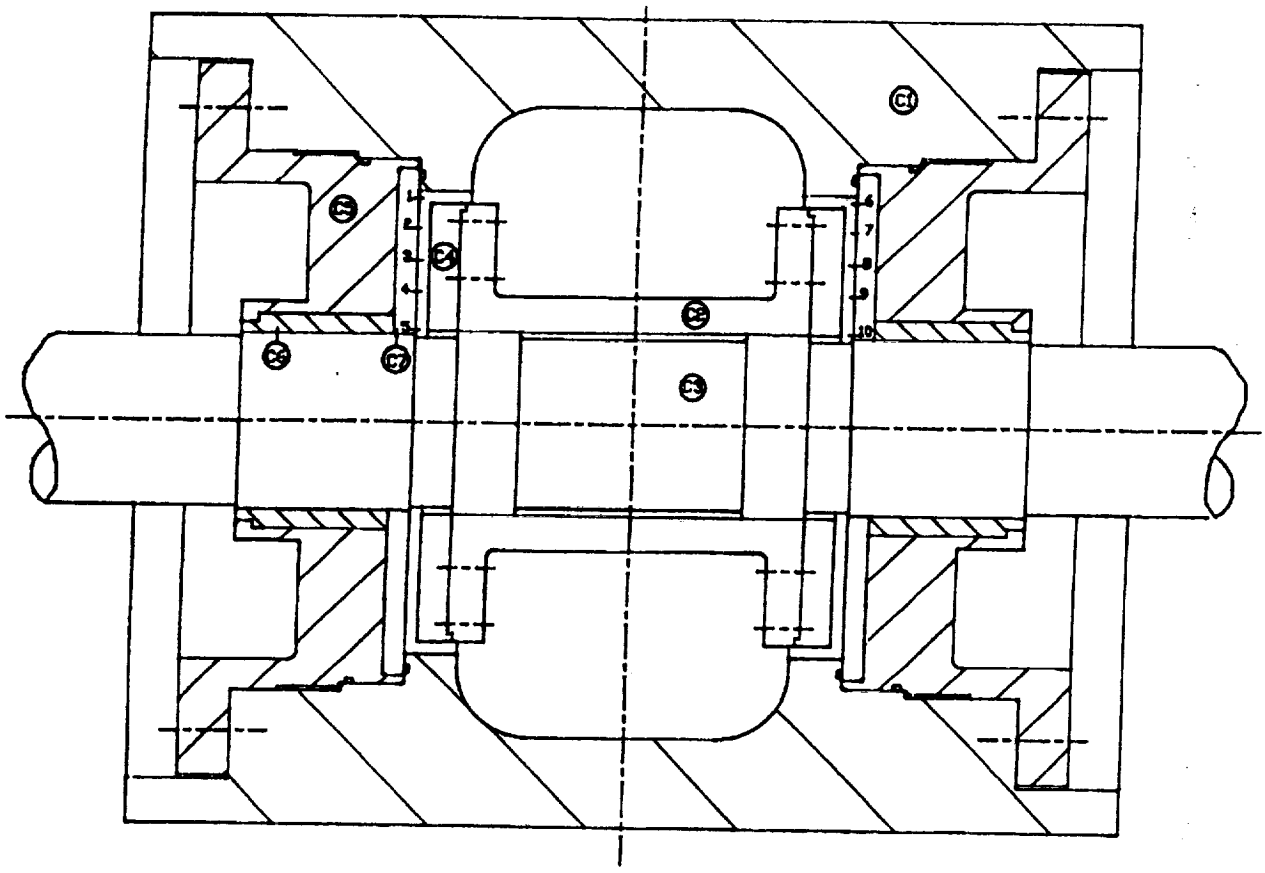

1-10 Static pressure tappings

C1 Casing
C2 Simulated impeller
C3 Rotor
C4 Plate for axial gap control
C5 Seal carrier
C6 Bronze sleeve
C7 anti-swirl plate

Figure 3 Cross-section of test seals

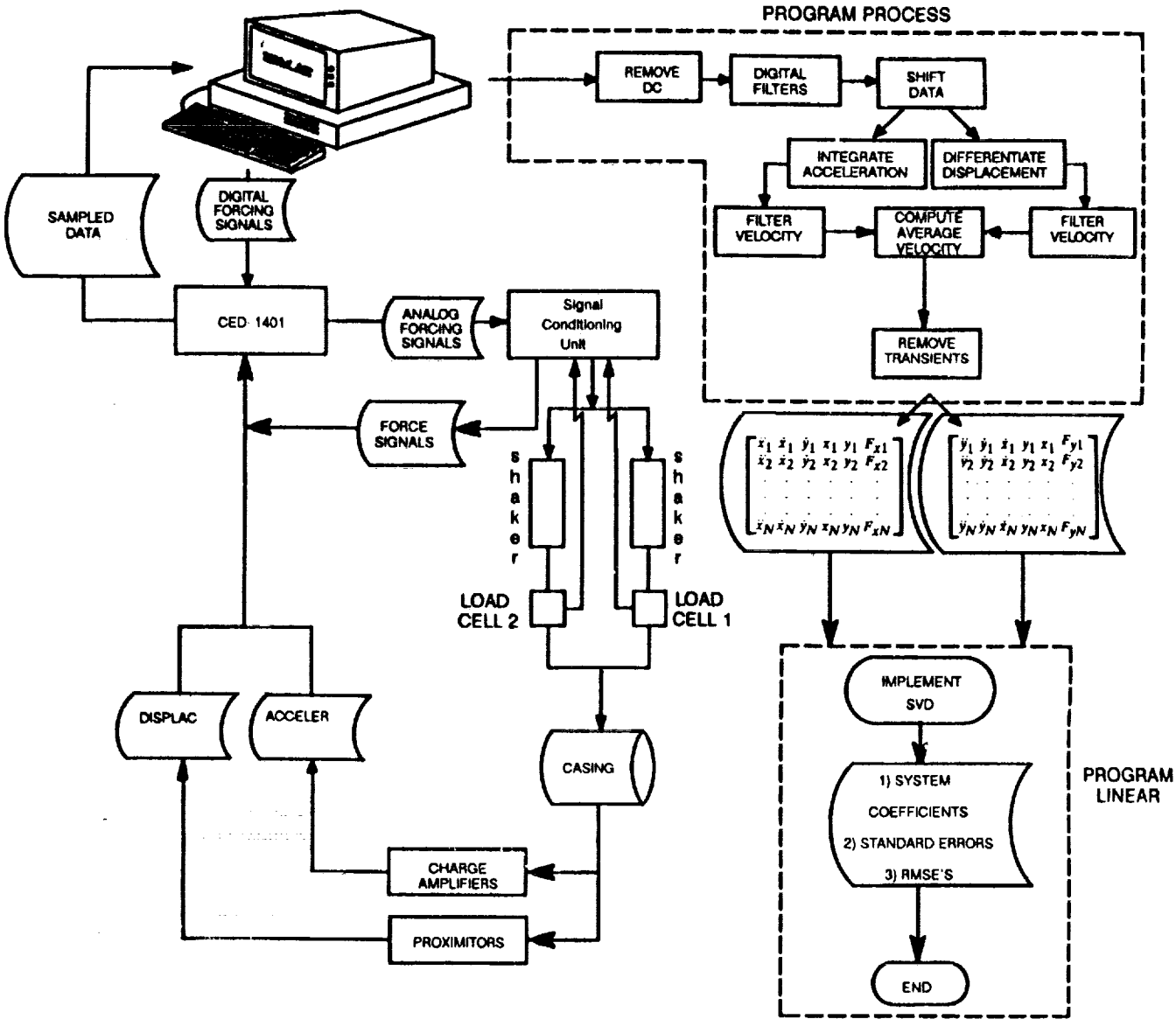

Figure 4 Data acquisition and reduction flow chart

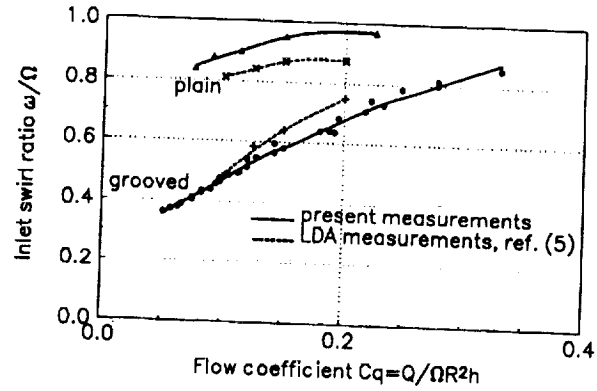

Figure 5 Inlet swirl ratio versus flow coefficient C_q

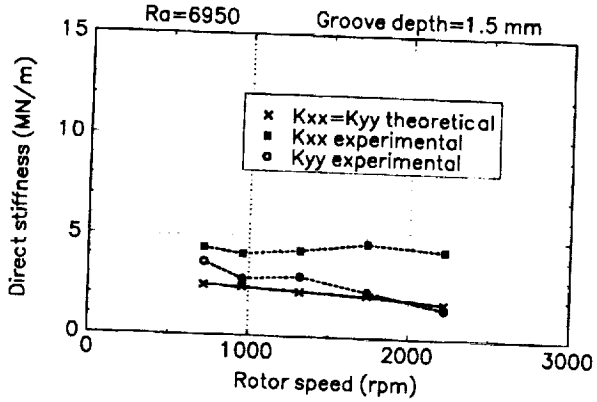

Figure 6.a Direct stiffness coefficients at R_a=6950

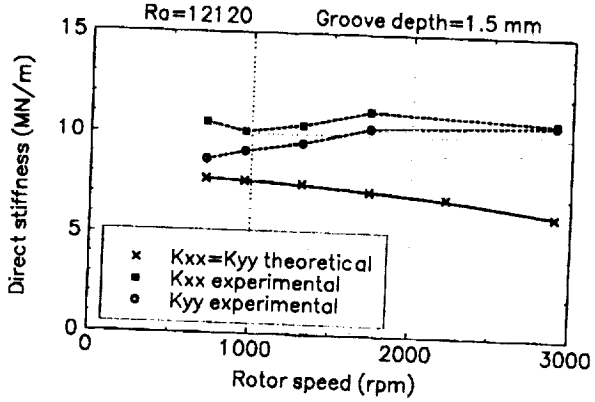

Figure 6.b Direct stiffness coefficients at R_a=12120

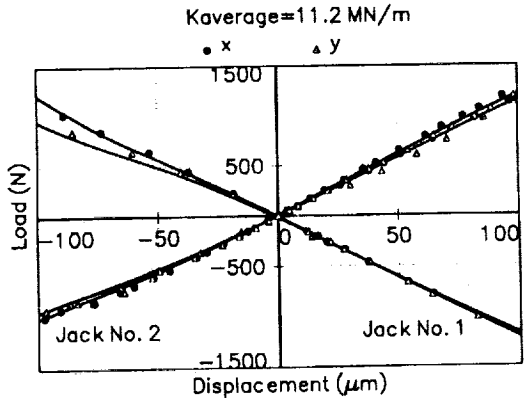

Figure 6.c Static stiffness of system at R_a=12100 and N=0 rpm

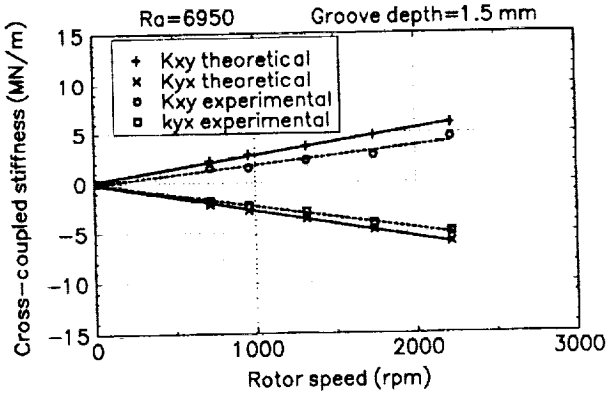

Figure 7.a Cross-coupled stiffness coefficients at R_a=6950

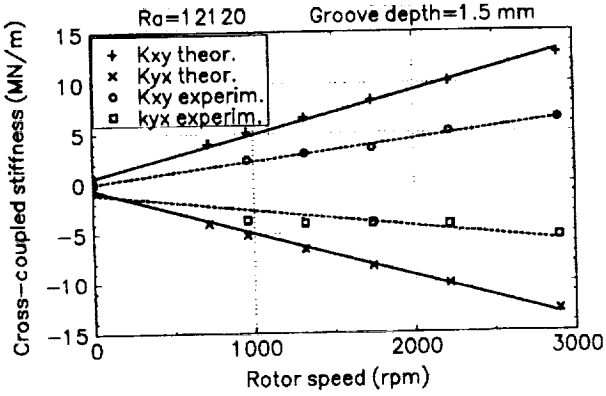

Figure 7.b Cross-coupled stiffness coefficients at R_a=12120

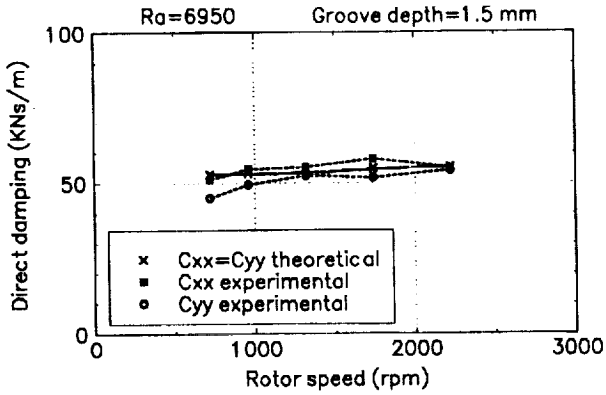

Figure 8.a Direct damping coefficients at R_a=6950

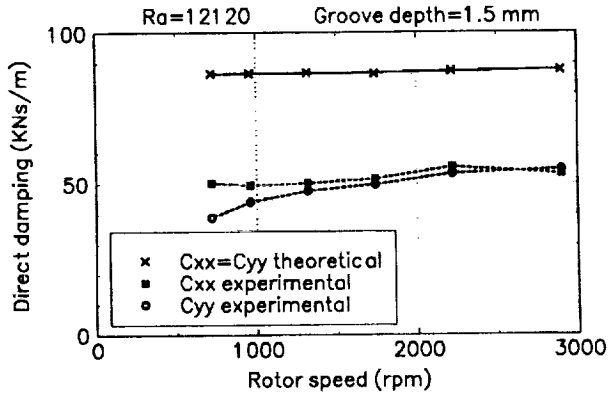

Figure 8.b Direct damping coefficients at R_a=12120

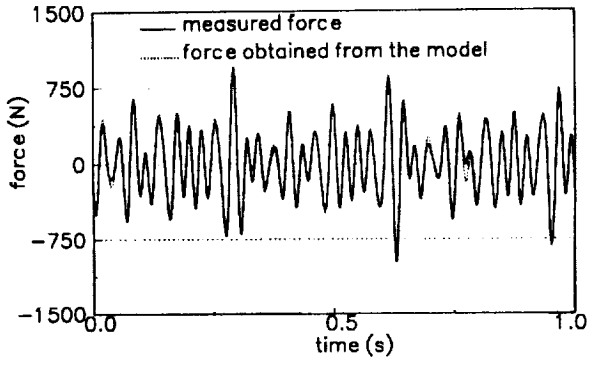

Figure 9 Comparison of measured and modelled forces